MIT Libraries | DSpace@MIT

MIT Open Access Articles

Exploring the Fe(III) binding sites of human serum transferrin with EPR at 275 GHz

The MIT Faculty has made this article openly available. ***Please share*** how this access benefits you. Your story matters.

Citation: Mathies, Guinevere, Peter Gast, N. Dennis Chasteen, Ashley N. Luck, Anne B. Mason, and Edgar J. J. Groenen. "Exploring the Fe(III) Binding Sites of Human Serum Transferrin with EPR at 275 GHz." JBIC Journal of Biological Inorganic Chemistry 20, no. 3 (December 24, 2014): 487–496.

As Published: http://dx.doi.org/10.1007/s00775-014-1229-z

Publisher: Springer Berlin Heidelberg

Persistent URL: http://hdl.handle.net/1721.1/107383

Version: Author's final manuscript: final author's manuscript post peer review, without publisher's formatting or copy editing

Terms of Use: Article is made available in accordance with the publisher's policy and may be subject to US copyright law. Please refer to the publisher's site for terms of use.

Massachusetts Institute of Technology

J Biol Inorg Chem manuscript No.
(will be inserted by the editor)

Exploring the Fe(III) binding sites of human serum transferrin with EPR at 275 GHz

Guinevere Mathies · Peter Gast · N. Dennis Chasteen · Ashley N. Luck · Anne B. Mason · Edgar J. J. Groenen

Received: date / Accepted: date

Abstract We report 275 GHz EPR spectra of human serum transferrin. At this high microwave frequency the zero-field splitting between the magnetic sublevels of the high-spin Fe^{3+} sites can be accurately determined. We find the zero-field splitting to be a sensitive probe of the structure of the transferrin iron-binding sites. Signals arising from iron bound to the transferrin N-lobe can clearly be distinguished from signals from iron bound to the C-lobe. Moreover, our spectra show that the structure of the iron site in the N-lobe is in-

Guinevere Mathies
Department of Physics, Huygens-Kamerlingh Onnes Laboratory, Leiden University, The Netherlands
Current address: Francis Bitter Magnet Laboratory, Department of Chemistry, Massachusetts Institute of Technology, Cambridge, MA 02139, United States, E-mail: mathies@mit.edu

Peter Gast
Department of Physics, Huygens-Kamerlingh Onnes Laboratory, Leiden University, The Netherlands

N. Dennis Chasteen
Department of Chemistry, Parsons Hall, University of New Hampshire, Durham, NH 03824, United States

Ashley N. Luck
Department of Biochemistry, University of Vermont College of Medicine, Burlington, VT 05405, United States

Anne B. Mason
Department of Biochemistry, University of Vermont College of Medicine, Burlington, VT 05405, United States

Edgar J. J. Groenen
Department of Physics, Huygens-Kamerlingh Onnes Laboratory, Leiden University, The Netherlands

fluenced by the presence and conformation of the C-lobe. The spectra of a series of N-lobe mutants altering the second-shell interaction of Arg124 with the synergistic anion carbonate reflect conformational changes induced at the iron site.

Keywords High-frequency EPR · High-spin Fe^{3+} · Human serum transferrin · zero-field splitting

1 Introduction

The transferrins are a family of iron-binding proteins that are found in a variety of biological fluids of all vertebrates, and also some invertebrates. [1,2] Iron is essential to life as it is a functional component of many proteins and enzymes. A major complication in the handling of iron is that ferric iron (Fe^{3+}) is insoluble, and can hydrolyze or reduce to ferrous iron (Fe^{2+}), which promotes the production of harmful radicals. Transferrins are able to bind ferric iron in a stable complex. They thereby serve to transport iron to cells and at the same time assure that no free iron is available to any other organism than the host.

The transferrin family has been studied extensively and a wealth of structural information is available. [3–7] Human serum transferrin (hTF) is an 80 kDa glycoprotein that consists, like most transferrins, of two homologous lobes, named the N- and C-lobe. Both lobes are able to bind one ferric iron inside a deep cleft. Release of iron is accompanied by a large conformational change in which the cleft opens around a hinge. [8] Four residues, which are conserved in vertebrates, coordinate to the iron: Asp63, Tyr95, Tyr188, and His249 (residue numbering for human serum isolated N-lobe), shown in Figure 1. The approximately octahedral coordination of the iron is completed by two oxygen atoms from the synergistic anion, carbonate, that binds together with the iron. The carbonate is kept in place by a network of hydrogen bonds to several amino acid residues, of which Arg124 is highly conserved.

Human serum transferrin sequesters Fe^{3+} avidly, with a binding constant in excess of 10^{20} M^{-1}. [10] Iron is released to cells through receptor mediated endocytosis. [11,12] Recent studies show that a lowering of the pH to 5.6, an unidentified chelator, and a series of interactions between both lobes and the receptor together orchestrate a fast, balanced release of the iron. [13–15] However, questions remain with regard to what happens locally at the iron site during iron release, although protonation of coordinating ligands appears to be crucial. [5,16–21] Iron is transported out of the endosome by a divalent metal transporter [2], which means that at some point ferric iron must be reduced to ferrous iron. Indirect

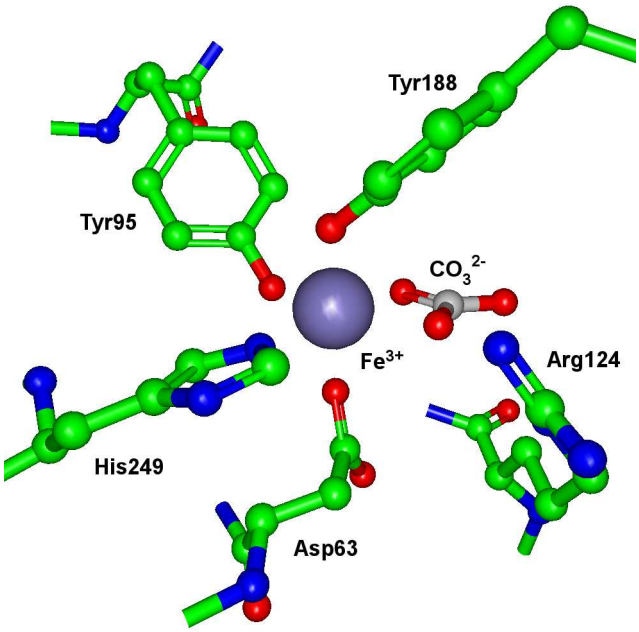

Fig. 1 The iron-binding site of human serum transferrin. The site shown is of isolated N-lobe, PDB ID 1A8E. [5] The image was created with Protein Workshop. [9] The carbonate and Arg124 are shown in conformation A, see Discussion.

evidence shows the involvement of ferrireductase Steap3; [22,23] however, the transferrin receptor may also raise the reduction potential of iron bound to human serum transferrin. [24] Experimental information on the electronic structure of the iron-binding site during the various steps in iron release would be most helpful in elucidating this process.

Electron paramagnetic resonance (EPR) spectroscopy probes the electronic structure of the iron binding site and thereby provides information on the nature of the iron in its bound state. The first 9.5 GHz (X band) EPR spectrum of hTF was reported in 1963 by Aasa *et al.*, [25] and by Windle *et al.* shortly thereafter. [26] However, because transferrin binds Fe^{3+} in the high-spin state ($S = 5/2$) and the six magnetic sublevels are split into three Kramers doublets by a zero-field splitting (ZFS) larger than the applied microwave quantum, EPR experiments at X band provide limited information. The ZFS parameters can merely be estimated and values reported by different laboratories show little agreement between them. [25,27–34] A large number of X-band spectra of transferrin are reported in the literature, but the use of these spectra to obtain structural information, or even their use as fingerprints, has been difficult (cf. Discussion). [10,29,31,35–47] A few EPR studies on transferrins at

higher microwave frequencies exist. At 34 GHz extremely complex spectra were obtained. [28] Even the combination of X-band and 95 GHz spectra did not allow a consistent interpretation. [48, 49] In Reference [50], a Minireview in this journal, a spectrum of human serum transferrin is reported at 285 GHz, but seemingly only as illustrative of high-frequency EPR of a biological high-spin Fe^{3+} center. The resolution, and thus the analysis, is limited and the authors do not distinguish contributions from the individual lobes.

Here we report continuous-wave (cw) EPR spectra at 275 GHz of human serum transferrin. Inter-doublet transitions are induced for the high-spin Fe^{3+} site of transferrin and therefore the 275 GHz spectra are rich in information. Small changes in the ZFS show up very distinctly, and the ZFS in turn is a sensitive probe of the structure of the high-spin iron sites.

We acquired 275 GHz spectra of human serum transferrin in several forms. First, wild-type human serum transferrin in which both lobes are loaded with iron (Fe2) was compared to authentic monoferric human serum transferrin, generated by disabling the iron-binding by a local mutation in either the C-lobe (FeN) or the N-lobe (FeC). The 275 GHz spectra of diferric human serum transferrin distinguishes signals from iron bound to the N-lobe from iron bound to the C-lobe, each iron having distinct ZFS parameters. Additionally, comparison of the spectra of Fe2, FeN and isolated N-lobe demonstrates that the presence and conformation of the C-lobe have an influence on the structure of the iron binding site in the N-lobe. Finally, we have studied three mutants of isolated N-lobe, in which Arg124 is either removed (R124A) or its conformation is altered (Y45E and L66W). The spectra reflect conformational changes induced at the iron site.

2 Materials and Methods

2.1 Human serum transferrin

Recombinant human serum transferrin (hTF) was expressed in baby hamster kidney cells using a pNUT expression vector. [51, 52] The recombinant hTF is non-glycosylated and contains an N-terminal hexa-histidine tag, but is functionally indistinguishable from hTF isolated from serum and containing two Asn-linked glycosylation sites. [53] Monoferric hTF was produced by disabling one of the binding sites by local mutations: monoferric C (FeC): N-His Y95F/Y188F hTF-NG, and monoferric N (FeN): N-His Y426F/Y517F hTF-

NG, as described in Reference [54]. Preparation of hTF/2N (N-lobe) mutants is described in detail in Reference [55]. The mutants R124A and Y45E were prepared using a polymerase chain reaction-based mutagenesis procedure. The L66W mutation was introduced using the Quik-Change mutagenesis kit (Stratagene). [16]

For the EPR experiments the protein was kept in 100 mM HEPES buffer at pH 7.4 at a concentration of $1-2$ mM. To ensure that iron loading was complete, no adventitious iron binding was taking place, and the iron-binding sites were intact, all samples were checked with UV/VIS absorption and X-band EPR spectroscopy. To shorten measurement time required for a good signal-to-noise ratio, the experiments on the mutants of isolated N-lobe were performed on highly concentrated samples. Protein solutions were concentrated to $5-10$ mM using a 30 kD molecular weight cut-off filter (Amicon). To assure that no changes in the spectra occurred due to dense packing of the protein and/or low water concentration, spectra were measured on isolated N-lobe wild type both at 1 mM and at 10 mM (compare Figures 3 and 7). No shifts of resonances were observed.

2.2 Continuous-wave EPR at 275 GHz

Continuous-wave (cw) 275.7 GHz EPR spectra were obtained on a spectrometer developed in our group, [56] using a probe dedicated to operation in cw mode. [57] Because a single-mode cavity was used to detect the EPR signal, only a very small sample volume of 20 nL was required. The applied microwave power was in the μW range. For the broad scans a modulation amplitude of 3 mT was used, the details of the $g \sim 2$ region were acquired with a modulation amplitude of 0.7 mT.

2.3 Data analysis

The EPR spectra of high-spin Fe^{3+}, $S = 5/2$, are interpreted using the spin Hamiltonian [58]

$$H = \mu_B \mathbf{B_0} \cdot \mathbf{g} \cdot \mathbf{S} + \mathbf{S} \cdot \mathbf{D} \cdot \mathbf{S}. \quad (1)$$

The ZFS tensor, **D**, is symmetric, can be taken traceless, and is characterized by two parameters, $D = 3/2D_z$ and $E = 1/2(D_x - D_y)$. The ratio E/D reflects the rhombicity of **D**. In the high-field limit, $\mathbf{S} \cdot \mathbf{D} \cdot \mathbf{S} \ll \mu_B \mathbf{B_0} \cdot \mathbf{g} \cdot \mathbf{S}$, the ZFS term may be treated as a perturbation to the Zeeman splitting. [59] As a result, a sample in which the spins are randomly oriented shows

a spectrum with equidistant signals with their spacing determined by the principal values of the ZFS tensor, D_i ($i = x,y,z$), according to

$$\Delta B_0 = \frac{3|D_i|}{\mu_B g_i} \tag{2}$$

Figure 2 shows the dependence of the magnetic sublevels of a $S = 5/2$ system in the high-field limit and the equidistant transitions for B_0 parallel to the principal axes of the ZFS tensor. At the lowest temperatures these transitions show up in the EPR spectra only above or below $g \sim 2$, depending on whether D_i is positive or negative, respectively (in our analysis we will follow the convention $|D_z| > |D_y| > |D_x|$). As the temperature is increased, sublevels higher in energy become populated and the corresponding transitions will become visible in the spectra. In particular in the region around $g \sim 2$ several transitions will start to show up close to each other, which are arranged in a complex pattern due to second-order effects.

Flexibility in the structure of a paramagnetic site leads to inhomogeneous line broadening in its EPR spectra. For high-spin Fe^{3+} complexes or proteins in frozen solution this shows up mainly as a strain in the ZFS, which can be remarkably large. [57, 60–62] Because a change in the ZFS brings about a change in resonance field that is proportional to m_s, the signals furthest away from the $g \sim 2$ region will be the most affected, see Figure 2. This leads to characteristic spectra with strong, narrow signals in the region around $g \sim 2$ (at 275.7 GHz this corresponds to 9.84 T) and weak, broad signals at the magnetic fields above and below the $g \sim 2$ region. [59]

In order to obtain a quantitative description of the high-spin Fe^{3+} spectra in terms of spin-Hamiltonian parameters, all spectra were simulated using the EPR simulation package EasySpin. [63] To reproduce the width and shape of the resonances, strain in D and E was taken into account by adding a Gaussian to the spectrum of a width proportional to the derivative of the resonance field with respect to D and E of a given transition.

3 Results

In Figure 3 the 275 GHz cw EPR spectra at 10, 15 and 20 K of the isolated N-lobe of human serum transferrin are shown. The broad, weak signals above and below the $g \sim 2$ region are emphasized in this figure, while the details of the narrow signals in the $g \sim 2$ region of the 10 K spectrum are shown in Figure 6. In the 10 K spectrum two broad, positive signals are observed at 8.44 T and 9.08 T. Two broad, negative signals show up at 10.78 T and around

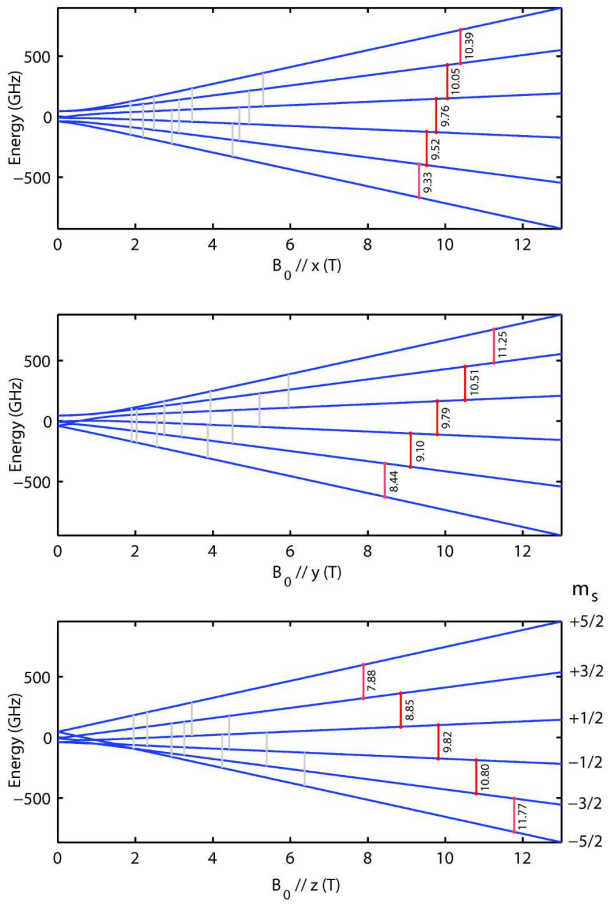

Fig. 2 The dependence of the energy of the six magnetic sublevels of a high-spin Fe^{3+} system, $S = 5/2$, on the magnitude of the magnetic field applied along the *x*, *y* and *z* principal directions of the g and ZFS tensors, which are assumed to be collinear. The ZFS and g tensor principal values determined from human serum transferrin N-lobe were used in this example, see Table 1. The vertical lines show 275.7 GHz resonance fields in Tesla. The light gray resonances have a negligible transition probability.

11.8 T. From the distance between each of these two signals D_y and D_z can be estimated to be -6.5 GHz and 9.2 GHz, respectively. This gives a value of -2.7 GHz for D_x. The 9.08 T peak shows a shoulder at 9.28 T and also at 9.49 T a signal shows up. We tentatively assign these signals to the absorption maxima ($B_0//x$) of the transitions between $|-5/2\rangle$ and $|-3/2\rangle$ and $|-3/2\rangle$ and $|-1/2\rangle$, respectively. Next to the 10.78 T signal a second, negative peak is visible at 10.56 T, which increases with temperature. We assign this peak to the high-field turning point between the sublevels $|+1/2\rangle$ and $|+3/2\rangle$ ($B_0//y$). Similarly a weak shoulder

at 8.83 T due to the low-field turning point ($B_0//z$) between the same sublevels becomes obvious at 20 K.

Simulation of the spectra of isolated N-lobe confirms our interpretation and allows fine tuning of the ZFS parameters. We find $D_z = 9.1$ GHz, $D_y =$ -6.6 GHz, and $D_x =$ -2.5 GHz, which corresponds to $D = 13.7$ GHz and $E = 2.1$ GHz, see Table 1. To reproduce the line widths, a strain in both D and E of 20 % was taken into account.

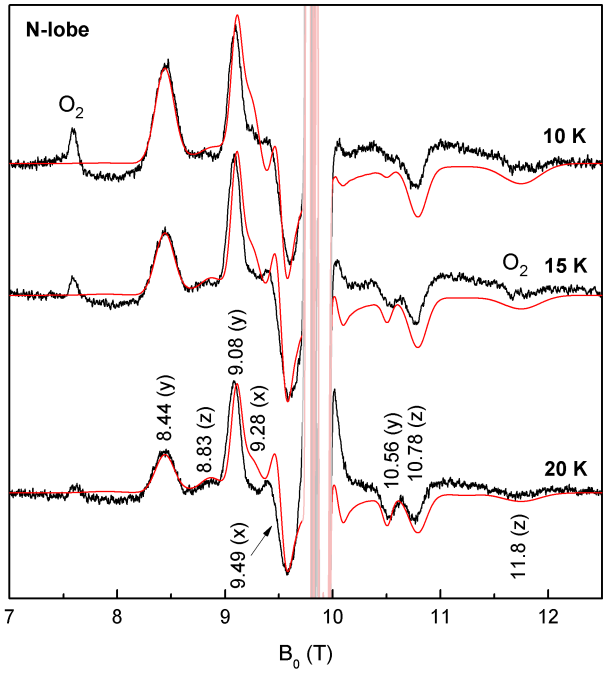

Fig. 3 275.7 GHz cw EPR spectra (black) and simulations (red) of the human serum transferrin N-lobe at 10, 15 and 20 K. The intense, narrow signals in the region around $g \sim 2$ are faded to bring forward the broad, weak signals above and below $g \sim 2$ and are shown in detail in Figure 6. Molecular oxygen is known to give signals at 7.6 and 11.7 T, which are marked in the spectra. [64] Simulation parameters are given in Table 1.

Figure 4 shows the 275 GHz EPR spectra of the monoferric mutants of human serum transferrin, FeC and FeN, which have high-spin Fe^{3+} bound only to the C-lobe or the N-lobe, respectively. Both spectra are typical for a high-spin Fe^{3+} in the high-field limit, but differ clearly in their ZFS parameters. An analysis similar to the analysis of the spectra from isolated N-lobe was performed on both the spectra from FeC and from FeN. The ZFS and strain parameters are shown in Table 1.

The spectrum of diferric human serum transferrin (Fe2) is shown in Figure 4 as well. Contributions from the N-lobe and the C-lobe are clearly resolved in this spectrum. Importantly, a simulation assuming a 60:40 contribution of FeC:FeN provides a good match with the experiment.

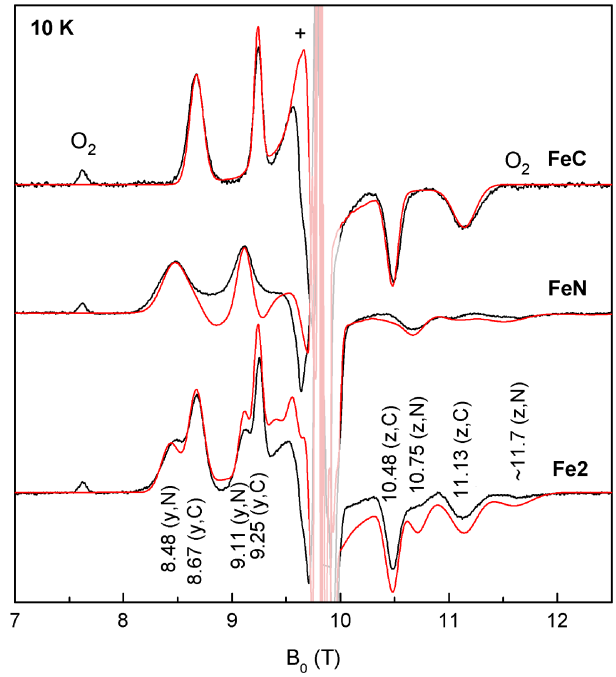

Fig. 4 275.7 GHz cw EPR spectra (black) and simulations (red) of the monoferric mutants of human serum transferrin (FeN) and (FeC) and diferric human serum transferrin (Fe2) at 10 K. The intense, narrow signals in the region around $g \sim 2$ are faded to bring forward the broad, weak signals above and below $g \sim 2$ and are shown in detail in Figure 6. An unknown impurity in the cavity generates a background signal around 9.6 T, marked with a $+$. Simulation parameters are given in Table 1.

Close inspection reveals that the signals arising from iron bound to the N-lobe differ for Fe2, FeN and isolated N-lobe. The high-field region of the EPR spectra above $g \sim 2$ is shown in more detail in Figure 5. The arrows mark the signal due to the $B_0//z$ turning point between the sublevels $|-3/2\rangle$ and $|-1/2\rangle$ for all three spectra at 10.72 T, 10.67 T, and 10.77 T, respectively. The corresponding $B_0//z$ turning points between the sublevels $|-5/2\rangle$ and $|-3/2\rangle$ around 11.8 T probably show corresponding variations, but these signals are too

shallow to allow a reliable measure. Thus, the values of D_z are different for Fe2(N), FeN, and isolated N-lobe: 8.4, 8.0, and 9.1 GHz, respectively.

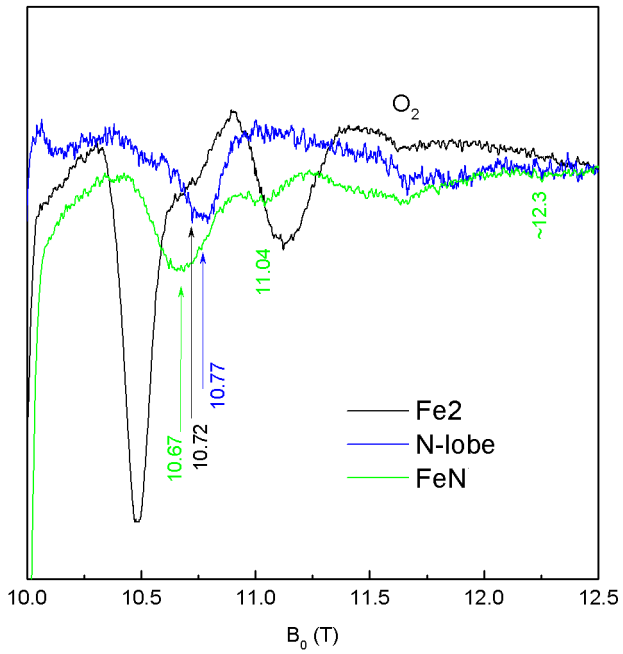

Fig. 5 Detail of the 275.7 GHz cw EPR spectra of the monoferric mutant of human serum transferrin (FeN), diferric human serum transferrin (Fe2), and N-lobe at 10 K.

Looking further at the spectrum of FeN in Figure 5, we see, in addition to the two signals at 10.67 T and around 11.6 T, two weaker signals at 11.04 T and around 12.3 T. These signals correspond to a high-spin Fe^{3+} site with a for transferrin remarkably large and axial ZFS ($D = 17.7$ GHz and $E/D = 0.03$). Thus, the spectrum of FeN shows a second high-spin Fe^{3+} site, likely a second conformation of the N-lobe iron-binding site. Signals due to this second conformation can be found in other parts of the 275 GHz spectra as well. Comparison of the regions below $g \sim 2$ for FeN and isolated N-lobe (compare Figure 3 and 4) shows two broad, positive peaks in both spectra at roughly the same field positions, but the line widths are larger for FeN - for the 8.44 T peak a FWHM of 0.23 T for isolated N-lobe and 0.32 T for FeN. The large line width in the FeN spectrum suggests that the value of D_y for the second conformation is different from the value of D_y for the first conformation (which is similar to that of isolated N-lobe), but that this difference is not resolved in the spectrum. The entire

spectrum of FeN can be well fitted taking into account two components with fractions 70% for conformation 1 and 30% for conformation 2 (see Table 1 for the fitting parameters), including the $g \sim 2$ region, shown in Figure 6. In particular, the signal at 9.73 T arises due to the high value of D_z of the second conformation.

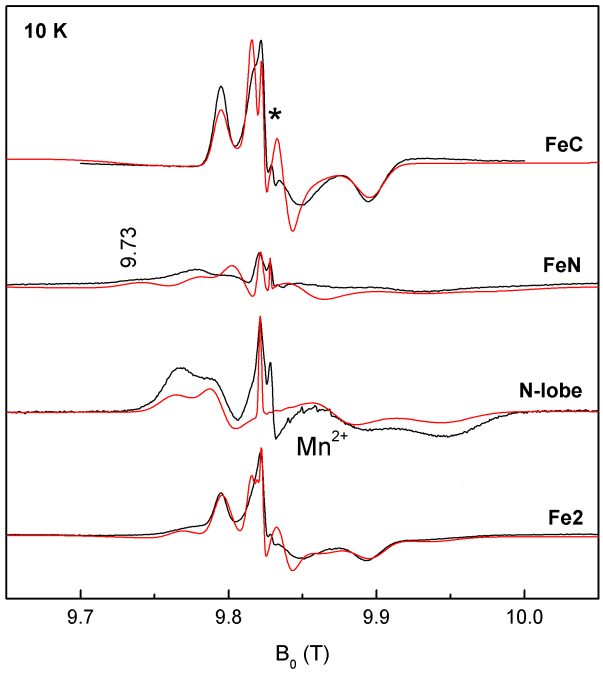

Fig. 6 The $g \sim 2$ region of the 275.7 GHz cw EPR spectrum (black) and simulation (red) of the human serum transferrin FeC, FeN, Fe2, and N-lobe at 10 K. A Mn^{2+} impurity is present around 9.85 T. A narrow signal of varying strength at 9.83 T ($g \sim 2$) is due to an impurity in the buffer, marked with a $\star$. Simulation parameters are given in Table 1.

Figure 6 shows also the $g \sim 2$ region of Fe2, FeC and isolated N-lobe and corresponding simulations. The spectrum of Fe2 is dominated by the contribution from the C-lobe, but also shows the signals arising from the N-lobe. The simulation of the Fe2 spectrum was performed assuming the same 60:40 fraction of FeC:FeN used to simulate the spectrum shown in Figure 4. Notably the $g \sim 2$ region of Fe2 does not show the signal at 9.73 T arising from the second conformation observed in the spectra of FeN.

We estimate the g values of the transferrin iron-binding sites to be around 2.004. The match between simulation and experiment in the $g \sim 2$ region is not sufficient to allow

us to determine the small deviations from g_e typically seen in high-spin Fe^{3+} sites with confidence. Specifically, the simulations reproduce the observed resonance fields, but not the intensities. This is probably related to the presence of g-strain, which deforms the spectra and was not taken into account in the simulations.

Table 1 Zero-field splitting parameters and strain used to simulate the human serum transferrin spectra shown in Figures 3, 4, 6, and 7. Line widths are expressed as full width at half maximum (FWHM) of the Gaussian distributions of D and E.

	D (GHz)	E (GHz)	E/D	D-strain %	E-strain %
Fe2 (N, 40%)	12.6	2.4	0.19	20	20
Fe2 (C, 60%)	9.3	2.4	0.25	18	18
FeN (1, 70%)	12.0	2.6	0.22	25	30
FeN (2, 30%)	17.7	0.6	0.03	20	20
FeC	9.3	2.4	0.25	18	18
N-lobe	13.7	2.1	0.15	20	20
N-lobe(R124A)	−11.6	−3.0	0.26	27	50
N-lobe(Y45E)	12.0	2.7	0.22	30	30
N-lobe(L66W)	13.1	2.4	0.18	25	25

We acquired 275 GHz spectra of three mutants of isolated N-lobe, in which Arg124 is either removed (R124A) or its conformation is altered (Y45E and L66W). In Figure 7 these spectra are compared to the spectrum of wild-type isolated N-lobe. The spectra of L66W and Y45E are similar to the wild type spectrum. The values of D_z are slightly smaller, 8.7 GHz for L66W and 8.0 GHz for Y45E as compared to 9.1 GHz for wild-type, while the values of D_y are the same. The Y45E spectrum shows an increase in the line width, e.g. from 0.23 T for isolated N-lobe (8.44 T peak) to 0.29 T for Y45E. The removal of Arg124 in the mutant R124A induces more drastic changes. The line widths in the spectrum have increased, e.g. to 0.5 T for the 8.2 T peak, which suggests a broad distribution of ZFS parameters or the presence of multiple conformations. The average values of D_z and D_y have changed to -7.7 and 6.8 GHz (the sign of D merely changes to adhere to the convention $|D_z| > |D_y| > |D_x|$).

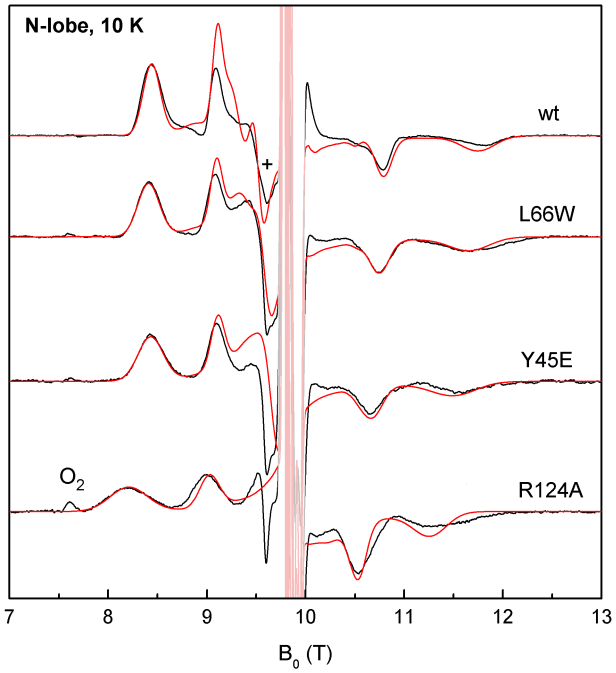

Fig. 7 275.7 GHz cw EPR spectra of the isolated N-lobe of human serum transferrin and the mutants of isolated N-lobe R124A, Y45E, and L66W at 10 K. The intense, narrow signals in the region around $g \sim 2$ are faded to bring forward the broad, weak signals above and below $g \sim 2$. An unknown impurity in the cavity generates a background signal around 9.6 T, marked with a $+$. Simulation parameters are given in Table 1.

4 Discussion

The vast majority of EPR spectra of transferrin reported in the literature are acquired at X band. The X-band EPR spectrum of transferrin shows two sets of signals, one around $g = 9$ and one around $g = 4.3$ arising from the $\pm 3/2$ doublet. The signal around $g = 4.3$ is broad, about 100 mT, and shows a characteristic shape. Selective iron loading revealed subtle differences in the X-band spectra between the C-lobe and the N-lobe. [10,35] Variations in the spectrum are also observed among transferrins from different organisms and other members of the transferrin family, including lactoferrin, ovotransferrin, and melanotransferrin. [29,36–38] Binding with a different synergistic anion and mutation of the coordinating ligands alters the spectrum drastically, [39,31,40–43] and also mutations further away from the iron-binding site are known to influence the spectrum, [44] as are salt concentration and pH. [45–47]

Despite many attempts, a satisfactory interpretation of the X-band spectrum of transferrin has not yet been provided. [27,28,30,33,34,65,49] Variations in the spectra are neither understood nor quantified, as in most cases they are merely changes in signal intensity that reshape the spectra and not shifts in resonance fields, which would be more informative. In this respect the analysis is strongly aided by performing EPR spectroscopy at a higher microwave frequency, thereby bringing the high-spin Fe^{3+} sites in the high-field limit. [59, 66] Inter-doublet transitions are resolved and the ZFS can be accurately determined.

In the 275 GHz cw EPR spectra of human serum transferrin, the signals from the iron ions in the two lobes are clearly distinguished. Comparison to the spectra of the monoferric mutants, FeN and FeC, made assignment possible to either the C-lobe or the N-lobe. Quantitative analysis of the 275 GHz spectra resulted in the determination of the ZFS parameters for the individual lobes: $D = 9.3$ GHz and $E/D = 0.25$ for C-lobe and $D = 12.6$ GHz and $E/D = 0.19$ for N-lobe of the diferric protein. It is noteworthy that these parameters have never previously been reported.

The ZFS parameters of the N- and C-lobe reveal a considerable difference in the electronic structure between the two iron-binding sites. This is consistent with studies of transferrin by biochemical methods. The two sites are known to differ in a number of properties, for example in the pH dependence of the iron-release rate, [67] even though the coordinating residues of the iron are the same and the geometries are similar. X-band EPR spectroscopy on transferrin substituted with Cu^{2+}, Cr^{3+}, and VO^{2+} showed differences in electronic structure between the two sites as well, [39,68,69] as did an ENDOR study of ^{57}Fe-transferrin. [70]

The high resolution of the 275 GHz spectra with respect to the ZFS made it possible to resolve small variations in the structure of the N-lobe iron-binding site. Comparison of the spectra of isolated N-lobe, Fe2, and FeN, reveals that the structure of the site in isolated N-lobe differs from the N-lobe site in monoferric FeN *and* in diferric Fe2. Thus, both the presence and the iron loading of the C-lobe have an influence on the N-lobe iron-binding site. X-ray diffraction on crystals of FeN bound to the transferrin receptor shows that the C2 subdomain, which undergoes a large rotation when the binding cleft opens, shows very little electron density, indicating that the unloaded C-lobe is highly mobile and disordered in the structure. As we find two distinct structures for the N-lobe site in FeN, which are both different from the structure of the N-lobe site in Fe2, it is not unthinkable that these

two conformations of the N-lobe are connected to an open conformation and a conformation intermediate between open and closed of the C-lobe.

We observe an influence of the C-lobe conformation on the N-lobe iron-binding site. However, we do not see the reverse effect, i.e., an influence of the N-lobe conformation on the C-lobe iron-binding site. Our spectra show no difference between the structures of the C-lobe sites in monoferric FeC and in diferric Fe2. These observations are in accord with results from kinetic studies of iron release by human serum transferrin. [13,71] i) The presence of the C-lobe slows the rate of iron release from the N-lobe. ii) Release from the N-lobe is impacted by the conformation of the C-lobe, but iron release from the C-lobe is not affected by the conformation of the N-lobe. A change in the release rate of iron in the N-lobe indicates, indirectly, a change in iron-binding site, which is readily seen in the electronic structure of the iron site as reflected in the different ZFS parameters for the N-lobe iron in the monoferric and diferric proteins (see Table 1).

The residue Arg124 is part of the hydrogen bond network that keeps the synergistic anion carbonate in place (see Figure 1) and is known to play a critical role in iron-binding and release. Molecular dynamics simulations show that upon protonation of Tyr188 the Arg124 swings away from the iron. [19,20] Mutation of Arg124 does not disable iron binding, but always leads to accelerated rates of iron release. [72,73]

The crystal structure of isolated N-lobe shows two conformations both for the synergistically bound carbonate anion and for the side chain of Arg124. [5] In conformation A the side chain of Arg124 is folded around the carbonate ion such that both the N_ε and NH_2 atoms are hydrogen bonded to the carbonate O_2 atom. The carbonate is bound in a slightly asymmetric, bidentate fashion to the iron. In conformation B the side chain of Arg124 is more extended and has moved away from the iron-binding site. The carbonate is still bidentate, but is more asymmetrically bound to the iron. Remarkably, the 275 GHz spectra of isolated N-lobe show no sign of the presence of a second conformation of the iron-binding site.

To investigate this more extensively we studied two mutants of isolated N-lobe, L66W and Y45E, which were designed to either push the Arg124 firmly against the carbonate, or pull it away, respectively, thereby mimicking the two conformations of Arg124 observed in the crystal structure of wild-type N-lobe. [16] Crystal structures obtained by X-ray diffraction confirmed the conformation of Arg124 in these two mutants. [16] In L66W the Arg124 is pressed firmly against the carbonate anion and a single conformation very similar to con-

formation A in wild-type is observed. In the crystal structure of Y45E, on the other hand, Arg124 is swung away from the carbonate and the position of the carbonate with respect to the iron is not well defined. These observations appear to be consistent with the 275 GHz spectra. The spectrum of L66W shows a single conformation with ZFS parameters that are slightly different from those of wild-type isolated N-lobe (see Table 1) and which may reflect a more stable A conformation with stronger H-bonding to Arg124. The 275 GHz spectrum of Y45E reveals a larger change in the ZFS parameters (see Table 1) and increased rhombicity ($E/D = 0.22$ vs. 0.15 for the wild-type isolated N-lobe) as well as an increase in line width from 0.23 T to 0.29 T, perhaps reflecting a less stable B conformation with greater disorder.

The 275 GHz spectra of Y45E and L66W clearly differ from each other, which makes it likely that the two conformations of carbonate and Arg124 observed in the crystal structure of isolated N-lobe would be resolved in our spectra or that, at least, an appropriate line broadening would be observed. However, the 275 GHz spectrum of isolated N-lobe is not a sum of the spectra of Y45E and L66W. We are therefore led to the conclusion that the two conformations are not present in our frozen solution of isolated N-lobe and that their observation by X-ray diffraction might be an artefact of crystallization.

Finally we investigated the N-lobe mutant R124A. [73, 74] X-ray diffraction data show severe changes to the iron-binding site upon removal of Arg124. The carbonate moves away from the arginine position by 0.3 Å and the iron atom moves with it away from liganding residues His249 and Asp63. The Fe-N(His) bond is thereby lengthened by approximately 0.3 Å to 2.4 Å. Notably the structure of the altered iron site of R124A is well defined. [75] The 275 GHz spectra show a large change in ZFS parameters for R124A, which indicates are correspondingly large change in structure. This may be related to the suggestion of Rinaldo *et al.* that for the R124A mutant, the His249 is protonated. [17, 18] The line width in the 275 GHz spectra of R124A has increased markedly to 0.5 T from 0.23 T for the wild-type, which suggests a pluriformity in the conformation of the iron site. The presence of multiple conformations is supported by the pH dependence of the iron-release, which follows a non-sigmoidal curve. [75] Thus, also for the N-lobe mutant R124A the global structural information obtained from the 275 GHz EPR spectra appears to be at variance with the crystal structure.

It would be of great interest if the observed ZFS parameters and the variation therein could be interpreted in terms of the structure of the transferrin iron-binding sites. Such a

translation would require an extensive quantum-chemical study and is challenging for high-spin d^5 systems, [76] but is the obvious next step towards understanding the iron binding by transferrin. However, even without knowledge of how they arise exactly, the ZFS parameters by themselves have turned out to be a valuable source of information. Because they are very sensitive to small changes in the structures of the metal sites, the ZFS parameters provide a way of identifying site-specific conformational states and, as such provide structural information relevant to function.

In our simulations of the 275 GHz EPR spectra we take the ZFS strain into account using a first order approximation. Although it was possible to analyze the spectra with this method, a complete match between experiment and simulation was not accomplished. i) The positions of the broad resonances above and below the $g \sim 2$ region are not reproduced exactly when one particular value of D_i is assumed. For example, of the two peaks at 8.44 T and 9.08 T in the spectra of wild-type isolated N-lobe (Figure 3), the peak at 9.08 T is not reproduced within 25 mT by a value of D_y of -6.6 GHz. ii) Scaling of the simulated spectrum to the experimental spectrum for one peak does not lead to proper scaling for other peaks. iii) Transition probabilities are not simulated properly in several cases. See for example the 9.28 T peak in the spectra of wild-type isolated N-lobe, Figure 3. To address these issues we are currently in the process of improving our method of simulating ZFS strain. This will be particularly important for the interpretation of the X-band spectra of transferrin, because in this situation $\mathbf{S}\cdot\mathbf{D}\cdot\mathbf{S} \gg \mu_B\mathbf{B_0}\cdot\mathbf{g}\cdot\mathbf{S}$ and the spectra are dominated by the distribution in E/D.

5 Conclusion

The question as to what comprises the EPR spectrum of transferrin has fascinated scientists for many decades. High-frequency EPR in conjunction with recombinant forms and mutants of human serum transferrin made it possible to determine the ZFS parameters characteristic of the iron ions bound to each of the two lobes, and thereby revealed a significant difference in structure. Moreover, an effect exerted by the presence and conformation of the C-lobe on the N-lobe iron-binding site was observed indirectly via small changes in the ZFS parameters of the iron ion bound to the N-lobe. Thus, the ability to determine the ZFS parameters of the individual lobes with high accuracy allowed us to answer a relevant biological ques-

tion. These findings show the power of high-frequency EPR in exploring the structure of the iron-binding sites of transferrin.

Acknowledgements The research was supported with financial aid by the Netherlands Organization for Scientific Research (NWO), Department of Chemical Sciences (CW). GM gratefully acknowledges the Rubicon Fellowship from the Netherlands Organization for Scientific Research.

References

1. P.F. Lindley, *Handbook of Metalloproteins* (Wiley & Sons, 2001), chap. Transferrins, pp. 793–811
2. P. Aisen, C. Enns, M. Wessling-Resnick, Int. J. of Biochem. Cell B. **33**, 940 (2001)
3. B.F. Anderson, H.M. Baker, G.E. Norris, D.W. Rice, E.N. Baker, J. Mol. Biol. **209**, 711 (1989)
4. H. Kurokawa, B. Mikami, M. Hirose, J. Mol. Biol. **254**, 196 (1995)
5. R.T.A. MacGillivray, S.A. Moore, J. Chen, B.F. Anderson, H. Baker, Y.G. Luo, M. Bewley, C.A. Smith, M.E. Murphy, Y. Wang, A.B. Mason, R.C. Woodworth, G.D. Brayer, E.N. Baker, Biochemistry **37**, 7919 (1998)
6. P.D. Jeffrey, M.C. Bewley, R.T.A. MacGillivray, A.B. Mason, R.C. Woodworth, E.N. Baker, Biochemistry **37**, 13978 (1998)
7. D.R. Hall, J.M. Hadden, G.A. Leonard, S. Bailey, M. Neu, M. Winn, P.F. Lindley, Acta Crystallogr. D. **58**, 70 (2002)
8. B.F. Anderson, H.M. Baker, G.E. Norris, S.V. Rumball, E.N. Baker, Nature **344**, 784 (1990)
9. J. Moreland, A. Gramada, O. Buzko, Q. Zhang, P. Bourne, BMC Bioinformatics **6**, 21 (2005)
10. P. Aisen, A. Leibman, J. Zweier, J. Biol. Chem. **253**, 1930 (1978)
11. R.D. Klausner, J. van Renswoude, G. Ashwell, C. Kempf, A.N. Schechter, A. Dean, K.R. Bridges, J. Biol. Chem. **258**, 4715 (1983)
12. P.K. Bali, O. Zak, P. Aisen, Biochemistry **30**, 324 (1991)
13. S.L. Byrne, N.D. Chasteen, A.N. Steere, A.B. Mason, J. Mol. Biol. **396**, 130 (2010)
14. B.E. Eckenroth, A.N. Steere, N.D. Chasteen, S.J. Everse, A.B. Mason, Proc. Nat. Acad. Sci. U.S.A. **32**, 13089 (2011)
15. A.N. Steere, N.D. Chasteen, B.F. Miller, V.C. Smith, R.T.A. MacGillivray, A.B. Mason, Biochemistry **51**, 2113 (2012)
16. T.E. Adams, A.B. Mason, Q.Y. He, P.J. Halbrooks, S.K. Briggs, V.C. Smith, R.T.A. MacGillivray, S.J. Everse, J. Biol. Chem. **278**, 6027 (2003)
17. D. Rinaldo, M.J. Field, Biophys. J. **85**, 3485 (2003)
18. D. Rinaldo, M.J. Field, Aust. J. Chem. **57**, 1219 (2004)
19. J.I. Mujika, X. Lopez, E. Rezabal, R. Castillo, S. Marti, V. Moliner, J.M. Ugalde, J. Inorg. Biochem. **105**, 1446 (2011)
20. J.I. Mujika, B. Escribano, E. Akhmatskaya, J.M. Ugalde, X. Lopez, Biochemistry **51**, 7017 (2012)
21. R. Kumar, A.G. Mauk, J. Phys. Chem. B **116**, 3795 (2012)

22. R.S. Ohgami, D.R. Campagna, E.L. Greer, B. Antiochos, A. McDonald, J. Chen, J.J. Sharp, Y. Fujiwara, J.E. Barker, M.D. Fleming, Nat. Genet. **37**, 1264 (2005)
23. A.K. Sendamarai, R.S. Ohgami, M.D. Fleming, C.M. Lawrence, Proc. Nat. Acad. Sci. U.S.A. **105**, 7410 (2008)
24. S. Dhungana, C.H. Taboy, O. Zak, M. Larvie, A.L. Crumbliss, P. Aisen, Biochemistry **43**, 205 (2004)
25. R. Aasa, B.G. Malmström, P. Saltman, T. Vänngård, Biochim. Biophys. Acta **75**, 203 (1963)
26. J.J. Windle, A.K. Wiersema, J.R. Clark, R.E. Feeney, Biochemistry **2**, 1341 (1963)
27. R.D. Dowsing, J.F. Gibson, J. Chem. Phys. **50**, 294 (1969)
28. R. Aasa, J. Chem. Phys. **52**, 3919 (1970)
29. R.A. Pinkowitz, P. Aisen, J. Biol. Chem. **247**, 7830 (1972)
30. R. Aasa, Biophys. Biochem. Res. Comm. **49**, 806 (1972)
31. P. Aisen, R.A. Pinkowitz, A. Leibman, Ann. New York Acad. Sci. pp. 337–346 (1973)
32. J.F. Gibson, J. Mol. Struc. **45**, 139 (1978)
33. M.I. Scullane, L.K. White, N.D. Chasteen, J. Magn. Reson. **47**, 383 (1982)
34. A.S. Yang, B.J. Gaffney, Biophys. J. **51**, 55 (1987)
35. D.A. Folajtar, N.D. Chasteen, J. Am. Chem. Soc. **104**, 5775 (1982)
36. S. Pollack, F.D. Lasky, Biophys. Biochem. Res. Comm. **70**, 533 (1976)
37. J.R. Gasdaska, J.H. Law, C.J. Bender, P. Aisen, J. Biol. Inorg. Chem. **64**, 247 (1996)
38. S. Farnaud, M. Amini, C. Rapisarda, R. Cammack, T. Bui, A. Drake, R. Evans, Y.S. Rahmanto, D.R. Richardson, Int. J. Biochem. Cell B. **40**, 2739 (2008)
39. P. Aisen, R. Aasa, B.G. Malmström, T. Vänngård, J. Biol. Chem. **242**, 2484 (1967)
40. J. Dubach, B.J. Gaffney, K. More, G.R. Eaton, S.S. Eaton, Biophys. J. **59**, 1091 (1991)
41. Q.Y. He, A.B. Mason, R.C. Woodworth, B.M. Tam, R.T.A. MacGillivray, J.K. Grady, N.D. Chasteen, Biochemistry **36**, 14853 (1997)
42. Q.Y. He, A.B. Mason, R. Pakdaman, N.D. Chasteen, B.K. Dixon, B.M. Tam, V. Nguyen, R.T.A. MacGillivray, R.C. Woodworth, Biochemistry **39**, 1205 (2000)
43. A.B. Mason, P.J. Halbrooks, N.G. James, S.A. Connolly, J.R. Larouche, V.C. Smith, R.T.A. MacGillivray, N.D. Chasteen, Biochemistry **44**, 8013 (2005)
44. A.B. Mason, P.J. Halbrooks, N.G. James, S.L. Byrne, J.K. Grady, N.D. Chasteen, C.E. Bobst, I.A. Kaltashov, V.C. Smith, R.T.A. MacGillivray, S.J. Everse, Biochemistry **48**, 1945 (2009)
45. E.M. Price, J.F. Gibson, J. Biol. Chem. **24**, 8031 (1972)
46. C.P. Thompson, B.M. McCarty, N.D. Chasteen, Biophys. Biochim. Acta **870**, 530 (1986)
47. J.K. Grady, A.B. Mason, R.C. Woodworth, N.D. Chasteen, Biochem. J. **309**, 403 (1995)
48. B.J. Gaffney, B.C. Maguire, R.T. Weber, G.G. Maresh, Appl. Magn. Reson. **16**, 207 (1999)
49. B.J. Gaffney, *Biological Magnetic Resonance 28 - High resolution EPR* (Kluwer Academic/Plenum Publishers, 2009), chap. 6. EPR of mononuclear non-heme iron proteins, pp. 233–268
50. K.K. Andersson, P.P. Schmidt, B. Katterle, K.R. Strand, A.E. Palmer, S.K. Lee, E.I. Solomon, A. Gräslund, A.L. Barra, J. Biol. Inorg. Chem. **8**, 235 (2003)
51. A.B. Mason, W.D. Funk, R.T.A. MacGillivray, R.C. Woodworth, Protein Expres. Purif. **2**, 214 (1991)
52. A.B. Mason, M.K. Miller, W.D. Funk, D.K. Banfield, K.J. Savage, R.W.A. Oliver, B.N. Green, R.T.A. MacGillivray, R.C. Woodworth, Biochemistry **32**, 5412 (1993)

53. A.B. Mason, Q.Y. He, P.J. Halbrooks, S.J. Everse, D.R. Gumerov, I.A. Kaltashov, V.C. Smith, J. Hewitt, R.T.A. MacGillivray, Biochemistry **41**, 9448 (2002)
54. A.B. Mason, P.J. Halbrooks, J.R. Larouche, S.K. Briggs, M.L. Moffett, J.E. Ramsey, S.A. Connolly, V.C. Smith, R.T. MacGillivray, Protein Expres. Purif. **36**, 318 (2004)
55. Q.Y. He, A.B. Mason, B.A. Lyons, B.M. Tam, V. Nguyen, R.T.A. MacGillivray, R.C. Woodworth, Biochem. J. **354**, 423 (2001)
56. H. Blok, J.A.J.M. Disselhorst, S.B. Orlinskii, J. Schmidt, J. Magn. Reson. **166**, 92 (2004)
57. G. Mathies, H. Blok, J.A.J.M. Disselhorst, P. Gast, H. van der Meer, D.M. Miedema, R.M. Almeida, J.J.G. Moura, W.R. Hagen, E.J.J. Groenen, J. Magn. Reson. **210**, 126 (2011)
58. A. Abragam, B. Bleaney, *Electron Paramagnetic Resonance of Transition Ions* (Dover Publications, New York, 1986)
59. A.L. Barra, A. Gräslund, K.K. Andersson, *Biological Magnetic Resonance 22 - Very high frequency (VHF) ESR/EPR* (Kluwer Academic/Plenum Publishers, 2004), chap. 5. The use of very high frequency EPR (VHF-EPR) in studies of radicals and metal sites in proteins and small inorganic models, pp. 145–163
60. J.T. Weisser, M.J. Nilges, M.J. Sever, J.J. Wilker, Inorg. Chem. **45**, 7736 (2006)
61. M. Benmelouka, J. van Tol, A. Borel, M. Port, L. Helm, L.C. Brunel, A.E. Merbach, J. Am. Chem. Soc. **128**, 7807 (2006)
62. G. Mathies, R.M. Almeida, P. Gast, J.J.G. Moura, E.J.J. Groenen, J. Phys. Chem. B **116**, 7122 (2012)
63. S. Stoll, A. Schweiger, J. Magn. Reson. **178**, 42 (2006)
64. L.A. Pardi, J. Krzystek, J. Telser, L.C. Brunel, J. Magn. Reson. **146**, 375 (2000)
65. B.J. Gaffney, H.J. Silverston, *Biological Magnetic Resonance 13 - EMR of paramagnetic molecules* (Plenum Press, New York, 1993), chap. 1. Simulation of the EMR spectra of high-spin iron proteins, pp. 1–57
66. J. Telser, J. Krzystek, A. Ozarowski, J. Biol. Inorg. Chem. **19**, 297 (2014)
67. J.V. Princiotto, E.J. Zapolski, Nature **255**, 87 (1975)
68. P. Aisen, R. Aasa, A.G. Redfield, J. Biol. Chem. **244**, 4628 (1969)
69. J.C. Cannon, N.D. Chasteen, Biochemistry **14**, 4573 (1975)
70. G.A. Rottman, K. Doi, O. Zak, R. Aasa, P. Aisen, J. Am. Chem. Soc. **111**, 8613 (1989)
71. S.L. Byrne, A.B. Mason, J. Biol. Inorg. Chem. **14**, 771 (2009)
72. O. Zak, P. Aisen, J.B. Crawley, C.L. Joannou, K.J. Patel, M. Rafiq, R.W. Evans, Biochemistry **34**, 14428 (1995)
73. H.R. Faber, C.J. Baker, C.L. Day, J.W. Tweedie, E.N. Baker, Biochemistry **35**, 14473 (1996)
74. Y. Li, W.R. Harris, A. Maxwell, R.T.A. MacGillivray, T. Brown, Biochemistry **37**, 14157 (1998)
75. H.M. Baker, Q.Y. He, S.K. Briggs, A.B. Mason, E.N. Baker, Biochemistry **42**, 7084 (2003)
76. C. Duboc, M.N. Collomb, F. Neese, Appl. Magn. Reson. **37**, 229 (2010)